Journal of
Materials Chemistry A

Accepted Manuscript

This is an *Accepted Manuscript*, which has been through the RSC Publishing peer review process and has been accepted for publication.

Accepted Manuscripts are published online shortly after acceptance, which is prior to technical editing, formatting and proof reading. This free service from RSC Publishing allows authors to make their results available to the community, in citable form, before publication of the edited article. This *Accepted Manuscript* will be replaced by the edited and formatted *Advance Article* as soon as this is available.

To cite this manuscript please use its permanent Digital Object Identifier (DOI®), which is identical for all formats of publication.

More information about *Accepted Manuscripts* can be found in the **Information for Authors**.

Please note that technical editing may introduce minor changes to the text and/or graphics contained in the manuscript submitted by the author(s) which may alter content, and that the standard **Terms & Conditions** and the **ethical guidelines** that apply to the journal are still applicable. In no event shall the RSC be held responsible for any errors or omissions in these *Accepted Manuscript* manuscripts or any consequences arising from the use of any information contained in them.

Table of content entry

PVA/CNF aerogels produced by an environmentally friendly freeze-drying process followed by thermal chemical vapor deposition of methyltrichlorosilane exhibit excellent oil and solvent absorption and remarkable heavy metal ion scavenging capability.

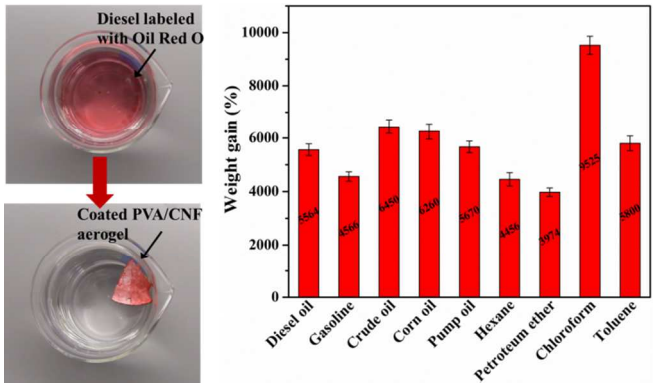

Green Synthesis of Polyvinyl Alcohol (PVA)–Cellulose Nanofibril (CNF) Hybrid Aerogels and Their Use as Superabsorbents

Qifeng Zheng,[a,b], Zhiyong Cai,[*,c] and Shaoqin Gong[**,a,b,d]

[a] *Material Science Program, University of Wisconsin–Madison, WI 53706, USA.*

[b] *Wisconsin Institute for Discovery, University of Wisconsin–Madison, WI 53715, USA*

[c] *Forest Product Laboratory, USDA, Madison, WI 53726, USA*

[d] *Department of Biomedical Engineering, University of Wisconsin–Madison, WI 53706, USA*

[*]Corresponding author: Zhiyong Cai. Email: zcai@fs.fed.us; Tel: +01 6082319446.
**Corresponding author: Shaoqin Gong. Email: sgong@engr.wisc.edu; Tel: +01 6083164311.

Abstract

Cross-linked polyvinyl alcohol (PVA)–cellulose nanofibril (CNF) hybrid organic aerogels were prepared using an environmentally friendly freeze-drying process. The resulting PVA/CNF aerogel was rendered both superhydrophobic and superoleophilic after being treated with methyltrichlorosilane via a simple thermal chemical vapor deposition process. Successful silanization on the surface of the porous aerogel was confirmed by various techniques including scanning electron microscopy (SEM), energy-dispersive X-ray analysis (EDS), Fourier transform infrared spectroscopy (FTIR), and contact angle measurements. The silane-treated, cross-linked PVA/CNF aerogels not only exhibited excellent absorption performance for various types of oil (e.g., crude oil) or organic solvents (with a typical weight gain ranging from 44 to 96 times of their own dry weight), but also showed a remarkable scavenging capability for several types of heavy metal ions tested (e.g., Pb^{2+}, Hg^{2+}), making it a versatile absorbent for various potential applications including water purification. Furthermore, these PVA/CNF aerogels demonstrated excellent elasticity and mechanical durability after silane-treatment as evidenced by the cyclic compression tests.

Introduction

Frequently occurring water pollution from oil and chemical spills/leaks as a result of accidents or natural disasters have resulted in a shortage of fresh water in many regions of the world. Water contaminants such as oil, organic solvents, and heavy metal ions can severely harm people and other living things.[1] Thus, there is a growing demand for innovative absorptive materials possessing high absorption capacity, high selectivity, and high efficiency.[1,2] Various types of absorption materials including cotton fibers,[3] carbon-based materials,[4-6] metal oxide nanowire-based composites,[2] and polymer-based materials[7,8] (e.g., polyester and polypropylene) have been

investigated in recent years. Among them, hydrophobic 3D porous materials appear to be the most promising class of high-capacity absorbents due to their light weight, high porosity, and large surface area, thus enabling them to rapidly absorb a large amount of oil and float on water.[4-6, 9-12] Nevertheless, several factors including complicated synthesis procedures and/or high cost of raw materials has limited their wide-spread application. Therefore, there is still a need to develop novel, sustainable/renewable, affordable, and robust high-capacity absorbent materials.

Here we demonstrate such a material that is produced via an environmentally friendly freeze-drying process,[13] i.e., a polyvinyl alcohol (PVA)–cellulose nanofibril (CNF) hybrid organic aerogel. Organic aerogels can exhibit many remarkable properties, including ultralow density (4–500 kg m^{-3}), high porosity, high specific surface area, and excellent mechanical properties (e.g., high modulus and high strength).[14-17] Cellulose is the most abundant and renewable natural polymer and is biocompatible and biodegradable.[18] Cellulose nanofibrils (CNFs) have high surface areas and high aspect ratios, thus they can easily form an entangled web-like structure.[19,20] CNFs can be fabricated using various methods including mechanical shearing,[21,22] 2,2,6,6,-tetramethylpiperidine-1-oxyl (TEMPO)-mediated oxidation,[23,24] enzymatic hydrolysis of macroscopic fibers followed by high-pressure homogenization,[25,26] or ultrasonication.[27,28] CNF aerogels usually exhibit ultralow densities, high surface areas, and reasonable mechanical properties.[29-31] They have been used in a wide range of applications, such as antibacterial agents,[32] thermal insulation[33] and oil absorbents.[34,35] PVA is an inexpensive polymer which possesses desirable properties such as water solubility, biocompatibility, and biodegradability.[36]

Superhydrophobic surfaces can generally be engineered by controlling the surface chemistry. For instance, it is known that silanization using judiciously selected silanes can lead to

superhydrophobic surfaces.[37-39] Silanes with hydrolyzable groups, such as chloride or alkoxide, react with water to form silanols, which can then react with other silanols or the hydroxyl groups present on the surface of solid materials (i.e., the PVA/CNF aerogels in this case), and may subsequently polymerize to form monolayers or silicone layers depending on specific reaction conditions.[38]

The PVA/CNF hybrid organic aerogels had very low densities (<15 kg m^{-3}) and very high porosities (>98%). The PVA/CNF aerogel became superhydrophobic and superoleophilic after being treated with methyltrichlorosilane using a simple thermal chemical vapor deposition process. The silane-coated PVA/CNF aerogels exhibited excellent absorption abilities for a variety of oils and organic solvents (ranging from 44 to 96 times their own dry weight), but strongly repelled water. Furthermore, the silane-treated PVA/CNF aerogels also showed a remarkable scavenging capability for heavy metal ions, making it a versatile absorbent medium for various applications. These aerogels also demonstrated excellent elasticity and high mechanical durability. Therefore, this study provides a simple and inexpensive method for fabricating robust superhydrophobic porous aerogels based on an abundant and renewable natural polymer (i.e., CNF), which possess desirable absorption and mechanical properties for oil and chemical spill/leak clean-up.

Experimental Section

Materials

The cellulose used for producing the CNFs was a commercially supplied fully bleached eucalyptus Kraft pulp. Polyvinyl alcohol (PVA, Mw~95000 g mol^{-1}), glutaraldehyde (GA, crosslinker, 25 wt.% in H_2O), 2,2,6,6-tetramethyl-1-piperidinyloxy (TEMPO, 98 wt.%), methyltrichlorosilane (99 wt.%), and Oil Red O were all obtained from Sigma–Aldrich. Sodium

chlorite, sodium bromide, sodium hypochlorite solution, and other chemicals were of laboratory grade (Fisher Scientific, USA) and used without further purification.

Preparation of CNFs

The TEMPO-oxidized CNFs used in this experiment were prepared according to a procedure described by Isogai's group.[40] Briefly, fully bleached eucalyptus fibers were oxidized with sodium hypochlorite using TEMPO as a catalyst at a temperature of 60 °C for 48 h. The fibers were then thoroughly washed and refined in a disk refiner with a gap of approximately 200 μm. The coarse fibers were separated by centrifuging at 12,000 G, and the fine CNF dispersion was then concentrated to 0.65 wt.% using ultrafiltration. A final refining step was performed in which the nanofiber dispersion was passed through an M-110EH-30 microfluidizer (Microfluidics, Newton, MA) once with 200- and 87-μm chambers in series. The resulting CNF suspension was stored at 4 °C without any treatment before future utilization. The carboxylate content of the CNFs was measured via titration based on the *TAPPI Test Method T237 cm-98* protocol and was found to be 0.64 mmol COONa per gram of CNFs.

Preparation of high density PVA solution

PVA (5.0 g, MW: 95000 g mol^{-1}) was dissolved in 100 mL of water and stirred for 12 h at 85℃ until the PVA was completely dissolved. Then, the PVA solution was used for the synthesis of aerogels.

Preparation of crosslinked PVA aerogels

PVA solution (4.0 mL, 0.05 g mL^{-1}) and a desired amount of water were mixed together in a flask under vigorous stirring for 1 h. Then, glutaraldehyde solution (80 μL, 25 wt.%) and sulfuric acid (80 μL, 1.0 vol%) were added to the PVA solution. The pH of the aqueous solution was controlled to be 4 to 6. The resulting mixture was mixed under stirring for another hour. At the

final stage, the mixture was sonicated in an ultrasonic bath for 1 h under vacuum to remove any bubbles. The resulting aqueous gel was transferred into aluminum pans and subsequently crosslinked in a vacuum oven at 75 ℃ for 3 h. Thereafter, a freeze-drying process was used to fabricate the PVA aerogel. Specifically, the crosslinked aqueous gel was precooled in a 4℃ refrigerator overnight to avoid macroscopic fracture during the freezing step. The precooled aqueous gel was then frozen at –78 ℃ in a dry ice–acetone solution and the resulting frozen sample was freeze-dried in a lyophilizer at a condenser temperature of –87.0 ℃ under vacuum (0.0014 mBar) for three days to produce the aerogel. The final aerogel products were stored in a vacuum oven for further characterization.

Preparation of crosslinked PVA/CNF aerogels

The PVA solution (2.0 mL, 0.05 g mL^{-1}), CNF solution (15.4 g, 0.65 wt.%), and a desired amount of water (depending on the specific density of the aerogels) were mixed together in a flask under vigorous stirring for 1 h. The weight ratio between the PVA and CNF was 1:1 for the PVA/CNF aerogels. Then, a glutaraldehyde solution (80 μL, 25 wt.%) and sulfuric acid (80 μL, 1.0 vol%) were added to the PVA/CNF solution.[41] The pH of the aqueous solution was controlled to be 4 to 6. The resulting mixture was mixed under constant stirring for another hour. At the final stage, the mixture was sonicated in an ultrasonic bath for 1 h under vacuum to remove any bubbles. The resulting aqueous gel was transferred into aluminum pans and was subsequently crosslinked/cured in a vacuum oven at 75 ℃ for 3 h. The PVA/CNF aerogel was obtained using the freeze-drying process described above and was stored in a vacuum oven for further characterization.

Preparation of superhydrophobic PVA/CNF aerogels

A thermal chemical vapor deposition (CVD) technique was developed for the surface modification of the PVA/CNF aerogels. A small glass vial containing methyltrichlorosilane (1 mL) was placed in a vacuum desiccator together with the aerogel samples and operated at 80 kPa below atmospheric pressure. The desiccator was sealed and heated in a vacuum-assisted oven at 50 ℃ for 12 h. To remove the excess amount of unreacted silane and the by-product (HCl), the surface-treated aerogels were kept in a vacuum desiccator under vacuum for more than 1 h.

Characterization

Unless stated otherwise, all tests described below were done in triplicate and the average results as well as the standard deviations were reported. The densities of the aerogels were calculated by measuring the mass and volume of the aerogels. The microstructure and elemental analyses of the aerogels were studied using a scanning electron microscope (SEM, LEO GEMINI 1530) equipped with energy-dispersive X-ray spectroscopy (EDX). The SEM samples were treated using gold sputtering. The Brunauer–Emmett–Teller (BET) specific surface area was determined by N_2 physisorption using a Gemini analyzer (Micromeritics, USA). It was measured by analyzing the amount of N_2 gas adsorbed on the samples with the relative vapor pressure (P/P_0) ranging from 0.05 to 0.3 at –196 ℃. A contact angle goniometer (OCA 15/20, Future Digital Scientific Corp., USA) was used for the water contact angle measurements at ambient temperature. The volume of the water droplet was fixed at 4.0 μL, and the contact angle was determined 10 s after the water droplet was deposited on the surface of the aerogel. The average value of five measurements performed at different surface locations was reported as the contact angle. The FTIR spectra were recorded on a Tensor 27 spectrometer (Bruker Daltonics Inc., USA) with 4 cm^{-1} resolution at room temperature. An inductively coupled plasma (ICP) atomic emission spectrometer (Optima 2000, PerkinElmer Inc., USA) was used for metal ions analysis

in aqueous solutions. Compression testing was conducted using an Instron (Model 5967) fitted with a 250 N load. The compression strain rate was set at 20% min^{-1} for the tests. Cylindrical aerogels (with a diameter of 60 mm and a height of 10 mm) were used for these compression testing. Thermal stability measurements were carried out using a thermogravimetric analyzer (TGA, Q 50 TA Instruments, USA) from 30 to 600 ℃ at a 10 ℃ min^{-1} heating rate under N_2 protection.

Oil/Solvent absorption capacity measurements

To measure the oil or solvent absorption of the aerogels, the silane-coated aerogels (~30 mg) were immersed into various types of oil (or solvent) and water with a 1:1 volume ratio except for chloroform. The chloroform absorption was measured by immersing the aerogel directly into the solvent because it has a higher density than water. The absorption process was very fast and generally reached equilibrium within a few minutes. Once the absorption was complete, the soaked aerogels were taken out and weighted after the aerogel surface was blotted using a filter paper to remove excess surface oil/solvent.[9] The absorption capacity (Q) was calculated from the mass gain using Equation 1,

$$Q\ (\%) = \frac{(W - W_0) \times 100\%}{W_0} \quad (1)$$

where W and W_0 were the weights of the aerogels before and after absorption, respectively. The weight measurements of the aerogels with absorbed oil were done quickly to avoid evaporation of the oil/solvent.

Heavy metal ion scavenging capacity measurements

The scavenging capacity of the aerogels on heavy metal ions including Pb^{2+}, Hg^{2+}, Ag^{+}, and Cu^{2+} were investigated. To measure the scavenging capacity, the silane-coated aerogels (~30 mg) and heavy metal ion solution (50 mL, 50 mg L^{-1}) were mixed under stirring at room temperature for 3

days to reach binding equilibrium. Before mixing, a few droplets of ethanol were applied onto the surfaces of the aerogels.[42] The heavy metal ion concentrations were measured with an ICP atomic emission spectrometer and the binding capacities of these heavy metal ions onto the aerogels were calculated using the Equation 2,

$$\text{Binding Capacity} = \frac{(C_{\text{I}} - C_{\text{eq}}) \times V}{M} \quad (2)$$

where C_I and C_{eq} (mg L^{-1}) were the initial and equilibrium concentrations of the heavy metal ions in aqueous solution, respectively, while V was the volume of the heavy metal ion solution (L), and M was the mass of the aerogels (g).

Results and Discussion

Silane coating of the aerogels

PVA/CNF aerogels, as well as the PVA aerogels used as a control, were successfully prepared using a freeze-drying method. Under optimal processing conditions, very little shrinkage was observed in these aerogels compared to their initial hydrogel dimensions. In order to obtain hydrophobic aerogels, the hydroxyl groups present on the porous surface of the aerogel were functionalized with methyltrichlorosilane in a gaseous phase through a simple thermal chemical vapor deposition method. The physical properties of aerogels with and without silane coating are summarized in Table 1. The densities of the PVA/CNF and PVA aerogels before and after the silane treatment were 10.6/13.0 kg m^{-3} and 11.7/14.2 kg m^{-3}, respectively. All aerogels exhibited a very high porosity (>98%). The porosity of aerogels was calculated using Equations S1 and S2. Fig. 1 shows the microstructures of the bottom surfaces of the PVA and PVA/CNF aerogels before and after silane coating. PVA and PVA/CNF aerogels before and after silane treatment all exhibited an interconnected, highly porous cellular structure with relatively uniform pore sizes

(typically 2 to 6 μm). In addition, more nanofiber-like structures appeared on the surface of the cellular wall (Fig. 1 (b) and (d)) after silanization, likely due to the formation of silicone nanofilaments.[36, 37] Previous studies have found that depending on the silane reaction conditions, different types of coating may be formed.[38,43,44] Under relatively dry conditions, organosilanes form either self-assembled monolayers (horizontal polymerization) or covalently attached monolayers. Under relatively wet conditions (i.e., with a relative humidity ranging from 35 to 65%), organosilanes form covalently attached cross-linked polymeric fibers/layers (vertical polymerization).[38,43,44]

Fig. 2 (c) and (d) show the microstructure of the PVA/CNF aerogel cross-sections at the middle of the aerogel samples before and after silane treatment. The PVA/CNF aerogels again exhibited a relatively uniform cellular structure with pore sizes typically in the range of 10 to 20 μm, which was several times larger than the pore sizes on the bottom surface. The bottom surface of the aerogels was in contact with the aluminum pan that was immersed in the dry ice–acetone solution. Differences in pore morphology between the bulk structure and the surface layers of aerogels were also reported in cellulose[29] and poly-(N-isopropyl acrylamide)/clay[45] aerogels fabricated using the freeze-drying process. However, similar to what was observed on the aerogel bottom surface, more nanofiber-like structures grew randomly on the PVA/CNF aerogel cellular walls, which was likely attributable to the formation of silicone nanofilaments (Fig. 2 (d)).[37,38]

Fig. 2 (a) and (b) show the microstructure of the PVA aerogel at the cross-section at the middle of the samples. Unlike the microstructure of the PVA/CNF aerogel cross-section, or that of the PVA aerogel bottom surface, the PVA aerogel cross-section largely exhibited a lamellar structure. This may be attributed to the fact that the precursor solution for the PVA aerogel had a

low viscosity, thereby allowing the PVA polymer chains to easily align along the direction of the growing front of ice crystals during freezing. In contrast, the PVA/CNF hydrogel solution used to prepare the PVA/CNF aerogel had a much higher viscosity due to the formation of a 3D network arising from the entanglement of high-aspect-ratio CNFs and thus may have affected the nucleation and growth of the ice crystals.[41] As shown in Table 1, the specific surface areas of the PVA/CNF aerogels was significantly higher than that of the PVA aerogels likely due to their small pore sizes as well as the high surface area possessed by CNFs.[19]

Successful silanization on the porous surface of the PVA/CNF aerogels was also confirmed by energy dispersive X-ray (EDX) analysis (Fig. 3). The EDX spectrum of the uncoated PVA/CNF aerogel showed carbon, oxygen, and sodium peaks, but no silicon peak was detected. After silanization, the EDX spectrum showed peaks for carbon, oxygen, sodium, chlorine, and silicon. The relative silicon atomic percentage by element was 4.44. A silicon mapping image shown in Fig. S1 indicated that the silane was uniformly coated on the porous surface of the aerogel. This was attributed to the high mobility of the reactive precursors in the gas phase, enabling them to easily penetrate through the porous structure of the aerogel.

Silanization of the porous PVA/CNF aerogels was further confirmed by FTIR analysis (Fig. 4). The absorption bands at ~780 cm^{-1} and ~1272 cm^{-1} were ascribed to the characteristic vibrations of Si–O–Si and C–Si asymmetric stretching in C–Si–O units, respectively.[12]

Surface wettability of the aerogels

The surface wettability of the PVA/CNF aerogel was studied via a contact angle measurement. As shown in Fig. 5 (a), for the uncoated PVA/CNF aerogels, water droplets were readily absorbed within 1 s, whereas the silane-coated aerogels became superhydrophobic (Fig. 5 (b)) as indicated by the very high contact angle ($\theta \approx 150.3 \pm 1.2°$ at t = 10 s). The water droplet

maintained its initial contact angle as well as its round shape on the silane-treated aerogel surfaces after 120 s.

When the superhydrophobic aerogel was immersed in water by applying an external force, the aerogel rose to the surface immediately after the external force was released, without absorbing any water. This implies that the superhydrophobic PVA/CNF aerogel can be used to absorb organic solvents or oil located on the surface of water. The silane-coated aerogels also exhibited a low adhesion to water. As shown in Fig. 5 (c), water droplets easily rolled off the surface of the PVA/CNF aerogel (cf. Movie S1 in the Supporting Information). In contrast, gasoline droplets were readily absorbed by silane-coated PVA/CNF aerogels (Fig. 5 (d), also cf. Movie S2 in the Supporting Information). Thus, the silane-coated PVA/CNF aerogels were highly oleophilic. The simultaneous superhydrophobicity and superoleophilicity exhibited by the silane-coated PVA/CNF aerogels ensures their superior oil/solvent absorbance.

Oil/Solvent absorption capacity of the aerogels

Removal of oils and organic contaminants from water has attracted immense academic and commercial interest because of the need to clean up industrial byproducts such as oily waste water and/or oil/chemical spills/leaks. The superhydrophobic and superoleophilic silane-coated PVA/CNF aerogel may be an ideal absorbent material for removing oil and organic solvents from water. The silane-coated PVA/CNF aerogels, which had a density of 13.0 kg m^{-3}, was used to investigate the oil absorption performance. Once a piece of the silane-coated aerogel was placed on the surface of the oil/solvent and water mixture, the oil/solvent was quickly absorbed by the aerogel within a few minutes, without absorbing water (Fig. 6 (a), also cf. Movie S3 in the Supporting Information). The oil/solvent (except chloroform due to its high density)-filled aerogel could be left floating on water essentially without any oil release or water absorption.

The absorption performance of the silane-coated PVA/CNF aerogels for different oils and organic solvents was measured and reported in Fig. 6 (b). The absorption capacities for a wide range of organic solvents and oils ranged from 44 to 96 times that of the aerogel's weight, which is much higher than most existing oil-absorption materials(cf. Table 2.[2,6,8-12, 46-48]). The excellent oil/solvent absorption capability exhibited by the PVA/CNF aerogel can be attributed to its highly porous structure as well as the uniform superoleophilic and superhydrophobic silane coating. The different absorption capacities observed among these oils and solvents were related to the densities of the respective oils or solvents, which could be normalized by dividing the oil/solvent weight gain by the density of the respective oil or organic solvent (Fig. 6 (c)). For comparison purposes, the oil/solvent absorption capacities of the silane-coated PVA aerogels with a similar density (14.2 kg m^{-3}) to that of the PVA/CNF aerogels were also measured and are presented in Fig. S2. The absorption capacities of the silane-coated PVA/CNF aerogels were two to three times higher than that of the silane-treated PVA aerogels, which may be attributed to the unique microstructure exhibited by the PVA/CNF aerogels that included more uniform and smaller pore sizes, higher surface area, and higher degrees of interconnection within their highly porous structures.

Heavy metal ion scavenging capability

Fig. 7 shows the heavy metal ion scavenging capacities of the PVA/CNF and PVA aerogels. The scavenging capacities of the PVA/CNF and PVA aerogels for Hg^{2+}, Pb^{2+}, Cu^{2+}, and Ag^{+} were 157.5 and 22.0 mg g^{-1}, 110.6 and 24.5 mg g^{-1}, 151.3 and 28.9 mg g^{-1}, and 114.3 and 39.5 mg g^{-1}, respectively. Clearly, the PVA/CNF nanocomposite aerogels demonstrated extremely high ion scavenging capacities, which were higher than the scavenging capacities of other materials reported in the literature,[44, 49, 50] as well as the PVA aerogel used as the control for this study. It is

believed that metal ion scavenging in aqueous solutions by porous materials such as aerogels is mainly driven by electrostatic interaction[51] and complexation between the metal ions and the carboxyl groups present in the porous materials.[51, 52] The CNFs used in the PVA/CNF aerogels carried a lot of carboxyl groups resulting from the TEMPO-oxidation process used to produce the CNFs. This may explain the much higher metal ion scavenging capability exhibited by the PVA/CNF aerogel in comparison to the PVA aerogel. As to the differences observed in the aerogel's scavenging capacities for different metal ions, this likely can be attributed to their different affinities to the carboxyl groups and probably other functional groups. The superior oil/solvent absorption performance coupled with the remarkable metal ion scavenging capabilities exhibited by the PVA/CNF aerogels makes them a versatile material for various applications such as water purification.

Thermal stability of the aerogels

The thermal stability of the PVA/CNF aerogels was measured before and after silane treatment by TGA in nitrogen from 30 to 600 °C and is shown in Fig. 8. Silane-coating did not change the thermal stability of the aerogels until around 270 °C. However, beyond 270 °C (up to 495 °C), the thermal stability of the silane-coated PVA/CNF aerogel was somewhat improved. For example, the temperatures corresponding to a 30% weight loss was 320.7 and 302.5 °C, for the silane-coated and uncoated PVA/CNF aerogels, respectively. This might be because the thermal decomposition of the aerogels was retarded by the silane coating on the porous surface of the PVA/CNF aerogel.[33]

Mechanical properties of the PVA/CNF aerogels

To study the mechanical properties of the silane-coated PVA/CNF aerogels, we measured their compressive stress as a function of strain as well as their cyclic compression behaviors (Fig. 9).

The PVA/CNF aerogels before and after silane-treatment can both be compressed by more than 90% because of their high porosity. However, before silane coating, the PVA/CNF aerogel was not very elastic and deformed permanently when the compression stain was more than 20%. Strikingly, the silane-coated PVA/CNF aerogel completely recovered their original shape with no mechanical failure after being subjected to 80% strain (Fig. 9 (a) and Movie S4 in the Supporting Information).

Fig. 9 (b) shows the cyclic compression stress–stain curve of the silane-treated PVA/CNF aerogels at a maxima strain of 40%, 60%, and 80%, respectively. The silane-coated aerogels completely recovered their original shapes after unloading at each strain. The maximal stress at 80% strain normalized by the density was found to be 3.8 ± 0.2 MPa cm^3 g^{-1}, which was higher than the values reported for other types of polymeric aerogels.[5,12,53,54] The silane-coated aerogels were subjected to a fatigue cyclic compression test (at 40%, 60%, and 80% strain) with 100 loading/unloading cycles (Fig. 9 (c), (d), and (e)). No obvious structural changes were observed after the cyclic compression test. The compressive stress–stain curves did not change significantly after 100 cycles, demonstrating excellent elastic recovery during the cyclic compression tests. Although hysteresis loops, which are an indication of dissipation, were seen in the loading–unloading cycles, the silane-coated PVA/CNF aerogels were significantly more elastic (40 to 80%) than other types of aerogels at comparable compression stains.

Conclusion

Superhydrophobic and superoleophilic PVA/CNF aerogels were produced by an environmentally friendly freeze-drying process followed by thermal chemical vapor deposition of methyltrichlorosilane. The silane-treated PVA/CNF hybrid aerogels had ultra-low densities (<15 kg m^{-3}), excellent oil/solvent absorption capabilities (44 to 96 times their own dry weight), and

remarkable metal ion scavenging capabilities, as well as superior elasticity and mechanical durability. Thus, the PVA/CNF aerogels made of renewable/ sustainable materials through simple and green processes may offer many promising applications including water purification to clean up oil/chemical spills/leaks and heavy metal contamination, thereby protecting our environment and all living species.

Acknowledgements

The authors gratefully acknowledge the financial support from the National Science Foundation (CMMI 1032186) and the USDA Forest Products Laboratory (Madison, WI). The authors are also thankful to Mr. Guojun Chen who helped to take the videos. The authors are also thankful to Professor Eric R. Roden for providing access to the BET surface area analyzer.

References

1 M. A. Shannon, P. W. Bohn, M. Elimelech, J. G. Georgiadis, B. J. Marinas and A. M. Mayes, *Nature*, 2008, **452**, 301–310.

2 J. Yuan, X. Liu, O. Akbulut, J. Hu, S. L. Suib, J. Kong and F. Stellacci, *Nat. Nanotechnol.*, 2008, **3**, 332–336.

3 G. Deschamps, H. Caruel, M. Borredon, C. Bonnin and C. Vignoles, *Environ. Sci. Technol.*, 2003, **37**, 10130–1015.

4 M. Toyoda and M. Inagaki, *Carbon*, 2000, **38**, 199–210.

5 H. Liang, Q. Guan, L. Chen, Z. Zhu, W. Zhang and S. Yu, *Angew. Chem. Int. Ed.*, 2012, **51**, 5101 –5105.

6 H. Bi, X. Xie, K. Yin, Y. Zhou, S. Wan, L. He, F. Xu, F. Banhart, L. Sun and R. S. Rouff, *Adv. Funct. Mater.*, 2012, **22**, 4421–4425.

7 J. Zhang and S. Seeger, *Adv. Funct. Mater.*, 2011, **21**, 4699–4704.

8 D. Ceylan, S. Doyu, B. Karacik, S. Yakan, O. Okay and O. Okay, *Environ. Sci. Technol.*, 2009, **43**, 3846–3852.

9 T. Wu, M. Chen, L. Zhang, X. Xu, Y. Liu, J. Yan, W. Wang and J. Gao, *J. Mater. Chem. A*, 2013, **1**, 7612–7621.

10 A. V. Rao, N. D. Hegde and H. Hirashima, *J. Colloid Interface Sci.*, 2007, **305**, 124–132.

11 J. T. Korhonen, M. Kettunen, R. H. A. Ras and O. Ikkala, *ACS Appl. Mater. Interfaces*, 2011, **3**, 1813–1816.

12 Q. Zhu, Y. Chu, Z. Wang, N. Chen, L. Lin, F. Liu and Q. Pan, *J. Mater. Chem. A*, 2013, **1**, 5386–5393.

13 H. Tamon, H. Ishizaka, T. Yamamoto and T. Suzuki, *Carbon*, 2000, **38**, 1099–1105.

14 D. Wu, F. Xu, B. Sun, R. Fu, H. He and K. Matyjaszewski, *Chem. Rev.*, 2012, **112**, 3959−4015.

15 C. Tan, B. M. Fung, J. K. Newman and C. Vu, *Adv. Mater.*, 2001, **13**, 644−646.

16 A. C. Pierre and G. M. Pajonk, *Chem. Rev.*, 2002, **102**, 4243−4265.

17 N. Hüsing and U. Schubert, *Angew. Chem., Int. Ed.*, 1998, **37**, 22−45.

18 D. Klemm, B. Heublein, H. Frink and A. Bohn, *Angew. Chem. Int. Ed.*, 2005, **44**, 3358–3393.

19 D. Klemm, F. Kramer, S. Moritz, T. Lindström, M. Ankerfors, D. Gray and A. Dorris, *Angew. Chem. Int. Ed.*, 2011, **50**, 5438–5466.

20 R. J. Moon, A. Martini, J. Nairn, J. Simonsen and J. Youngblood, *Chem. Soc. Rev.*, 2011, **40**, 3941–3994.

21 D. O. Carlsson, G. Nyström, Q. Zhou, L. A. Berglund, L. Nyholm and M. Strømme, *J. Mater. Chem.*, 2012, **22**, 19014–19024.

22 S. Iwamoto, K. Abe and H. Yano, *Biomacromolecule*, 2008, **9**, 1022–1026.

23 T. Saito, S. Kimura, Y. Nishiyama and A. Isogai, *Biomacromolecules*, 2007, **8**, 2485–2491.

24 T. Saito, M. Hirota, N. Tamura, S. Kimura, H. Fukuzumi, L. Heux and A. Isogai, *Biomacromolecules*, 2009, **10**, 1992–1996.

25 M. Paakko, M. Ankerfors, H. Kosonen, A. Nykanen, S. Ahola, M. Osterberg, J. Ruokolainen, J. Laine, P. T. Larsson, O. Ikkala and T. Lindstrom, *Biomacromolecules*, 2007, **8**, 1934–1941.

26 M. Henriksson, G. Henriksson, L. A. Berglund and T. Lindstrom, *Eur Polym J.*, 2007, **43**,3434–3441.

27 P. C. S. F. Tischer, M. R. Sierakowski, H. Westfahl and C. A. Tischer, *Biomacromolecules*, 2010, **11**, 1217–1224.

28 L. Wågberg, G. Decher, M. Norgren, T. Lindström, M. Ankerfors and K. Axnäs, *Langmuir*, 2008, **24**, 784–795.

29 H. Sehaqui, M. Salajkova, Q. Zhou and L. A. Berglund, *Soft Matter*, 2010, **6**, 1824–1832.

30 W. Chen, H. Yu, Q. Liu, Y. Liu and J. Li, *Soft Matter*, 2011, **7**, 10360–10368.

31 M. Pääkkö, J. Vapaavuori, R. Silvennoinen, H. Kosonen, M. Ankerfors, T. Lindström, L. A. Berglund and O. Ikkala, *Soft Matter*, 2008, **4**, 2492–2499.

32 I. Díez, P. Eronen, M. Österberg, M. B. Linder. O. Ikkala and R. H. A. Ras, *Macromol. Biosci.*, 2011, **11**, 1185–1191.

33 A. Javadi, Q. Zheng, F. Payen, A. Javadi, Y. Altin, Z. Cai, R. Salo and S. Gong, *ACS Appl. Mater. Interfaces*., 2013, **5**, 5969–5975

34 M. Kettunen, R. J. Silvennoinen, N. Houbenov, A. Nykänen, J. Ruokolainen, J. Sainio, V. Pore, M. Kemell, M. Ankerfors, T. Lindström, M. Ritala, R. H. A. Ras and O. Ikkala, *Adv. Funct. Mater.*, 2011, **21**, 510–517.

35 J. T. Korhonen, M. Kettunen, R. H. A. Ras and O. Ikkala, *ACS Appl. Mater. Interfaces*, 2011, **3**, 1813–1816.

36 S. Matsumura, H. Kurita and H. Shimokobe, *Biotechnol Lett.*, 1993, **15**, 749–754.

37 J. Zhang and S. Seeger, *Adv. Funct. Mater.*, 2011, **21**, 4699–4704

38 G. R. J. Artus, S. Jung, J. Zimmermann, H. Gautschi, K. Marquardt and S. Seeger, *Adv. Mater.*, 2006, **18**, 2758–2762

39 M. Jin, J. Wang, X. Yao, M. Liao, Y. Zhao and L. Jiang, *Adv. Mater.*, 2011, **23**, 2861–2864.

40 T. Saito, M. Hirota, N. Tamura, S. Kimura, H. Fukuzumi, L. Heux and A. Isogai, *Biomacromolecules*, 2009, **10**, 1992–1996.

41 Q. Zheng, A. Javadi, R. Sabo, Z. Cai and S. Gong, *RSC Adv.*, 2013, **3**, 20816–20823.

42 Z. Sui, Q. Meng, X. Zhang, R. Ma and B. Cao, *J. Mater. Chem.*, 2012, **22**, 8767–8771.

43 A.Y. Fadeev and T.J. McCarthy, *Langmuir*, 2000, **16**, 7268–7274.

44 M. A. Shirgholami, M. S. Shalil-Abad, R. Khajavi and M. E. Yazdanshenas, *Journal of Colloid and Interface Science*, 2011, **359**, 530–535.

45 K. Haraguchi and K. Matsuda, *Chem. Mater.*, 2005, **17**, 931–934.

46 S. Tao, Y. Wang and Y. An, *J. Mater. Chem.*, 2011, **21**, 11901–11907.

47 A. Li, H. Sun, D. Tan, W. Fan, S. Wen, X. Qing, G. Li, S. Li and W. Deng, *Energy Environ. Sci.*, 2011, **4**, 2062–2065.

48 S. Choi, T. Kwon, H. Im, D. Moon, D. J. Baek, M. Seol, J. P. Duarte and Y. Choi, *ACS Appl. Mater. Interfaces*, 2011, **3**, 4552–4556.

49 T. S. Sreeprasad, S. M. Maliyekkal, K. P. Lisha and T. Pradeep, *Journal of Hazardous Materials*, 2011, **186**, 921–931

50 L. Carro, R. Herrero, J. L. Barriada and M. E. Sastre de Vicente, *J Chem Technol Biotechnol*, 2009, **84**, 1688–1696

51 A.M. Liu, K. Hidajat, S. Kawi and D. Y. Zhao, *Chem. Commun.*, 2000, **13**, 1145–1146.

52 M. Benitez, D. Das, R. Ferreira, U. Pischel and H. Garcia, *Chem. Mater.*, 2006, **18**, 5597–5603.

53 L. J. Gibson and M. F. Ashby, *Cellular Solids: Structure and Properties*, Cambridge Univ. Press, Cambridge, England 1997.

54 M. D. Gawryla, O. van den Berg, C. Weder and D. A. Schiraldi, *J. Mater. Chem.*, 2009, **19**, 2118–2124.

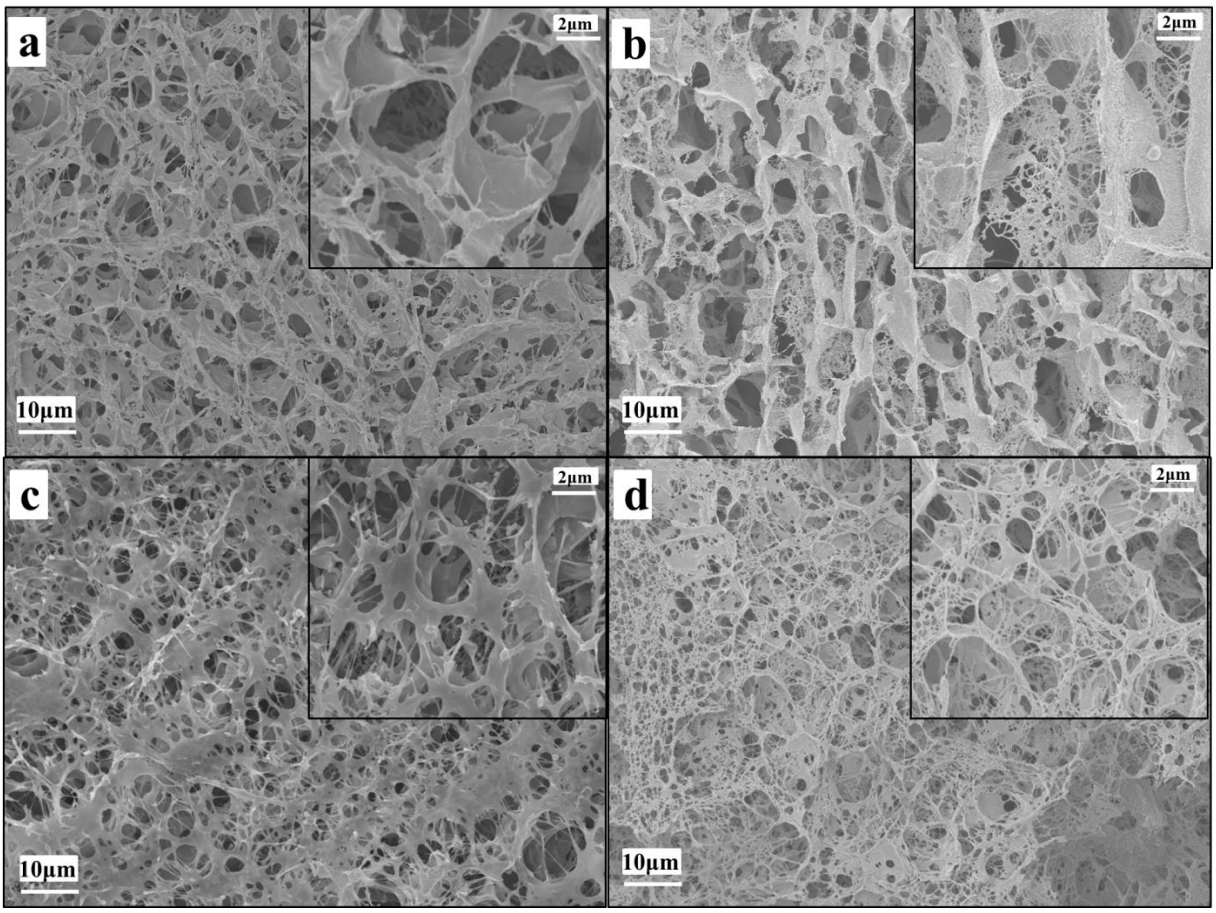

Fig. 1 SEM images of the bottom surface of the aerogels: (a) uncoated PVA aerogel, (b) coated PVA aerogel, (c) uncoated PVA/CNF aerogel, and (d) coated PVA/CNF aerogel.

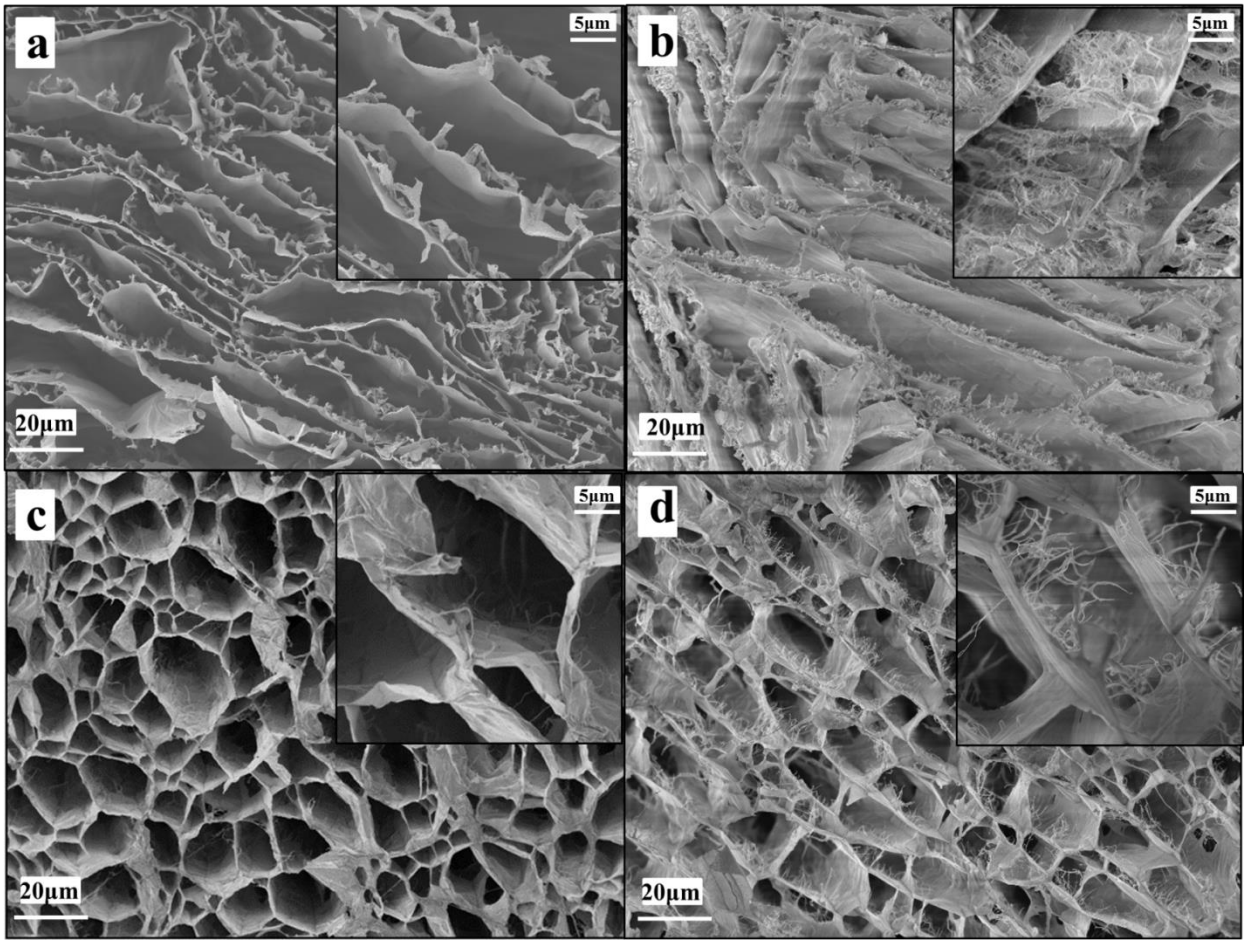

Fig. 2 SEM images of the cryofractured surfaces of aerogels: (a) uncoated PVA aerogel, (b) coated PVA aerogel, (c) uncoated PVA/CNF aerogel, and (d) coated PVA/CNF aerogel.

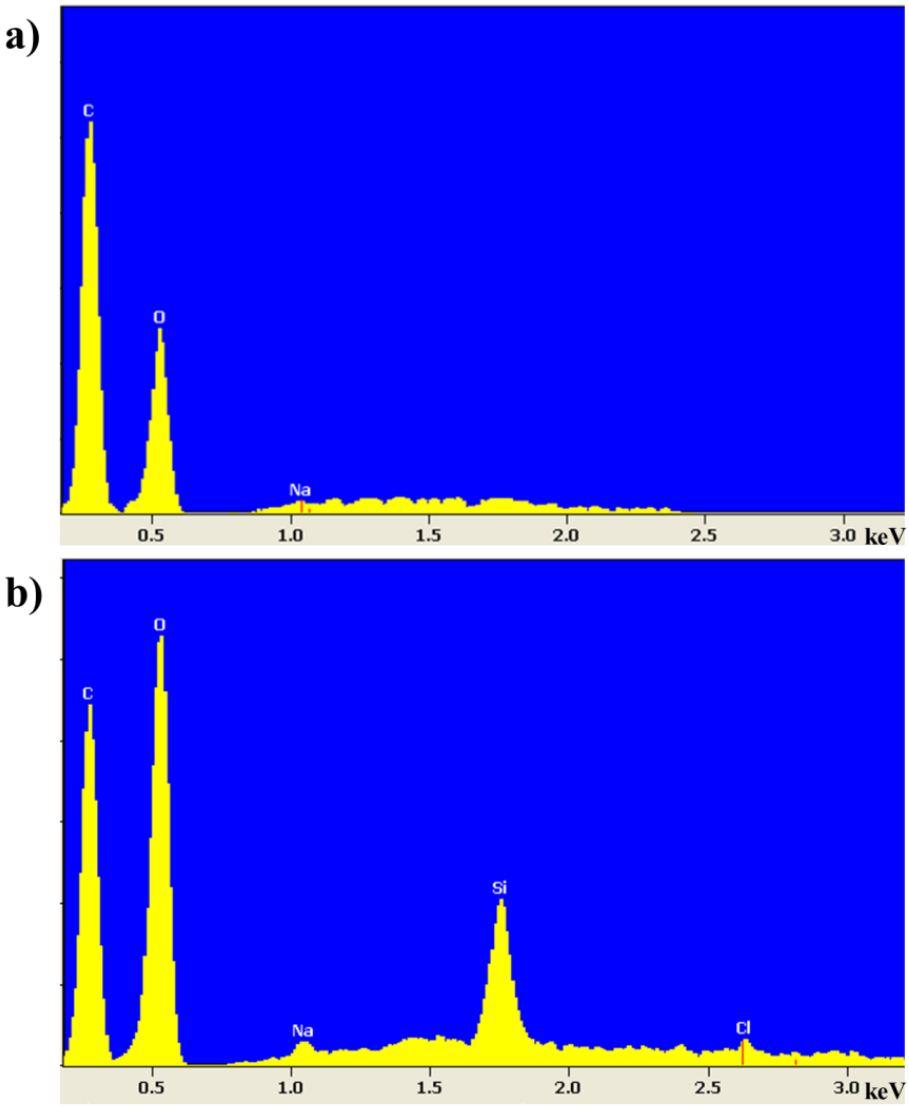

Fig. 3 EDX spectra of the PVA/CNF aerogels: (a) uncoated aerogel, and (b) coated aerogel.

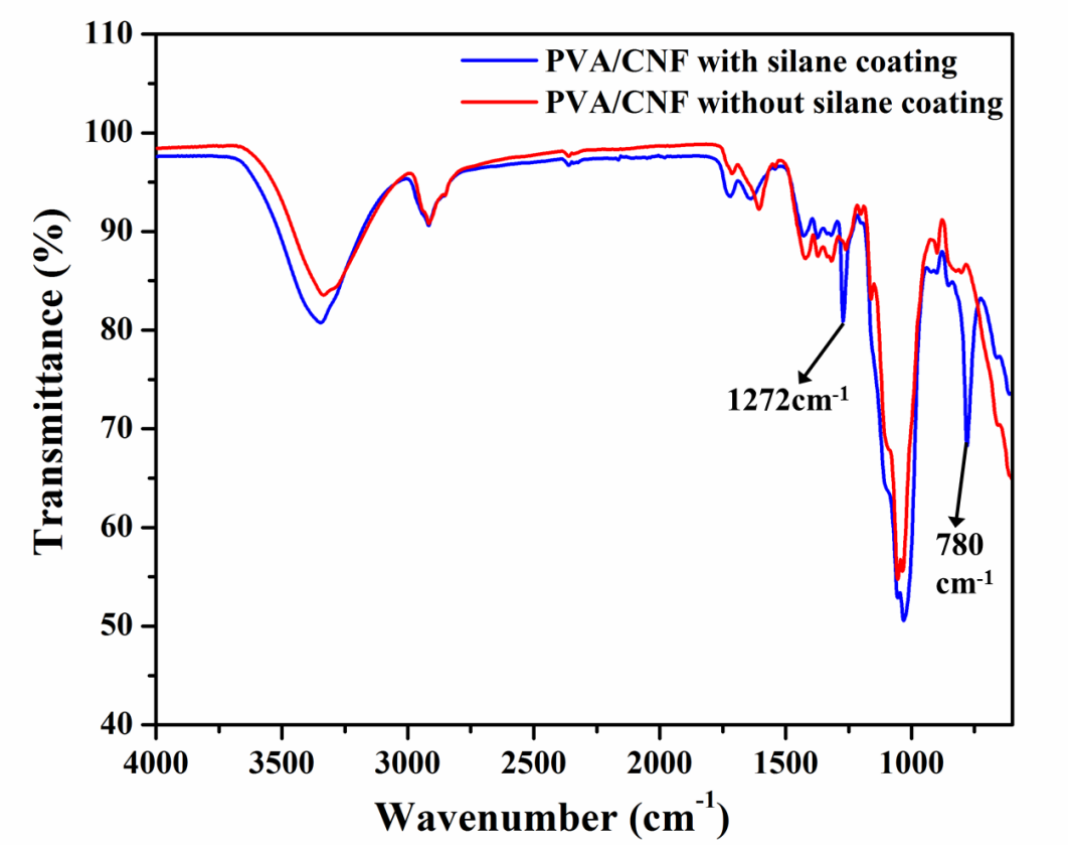

Fig. 4 FTIR spectra of PVA/CNF aerogels with and without silane coating.

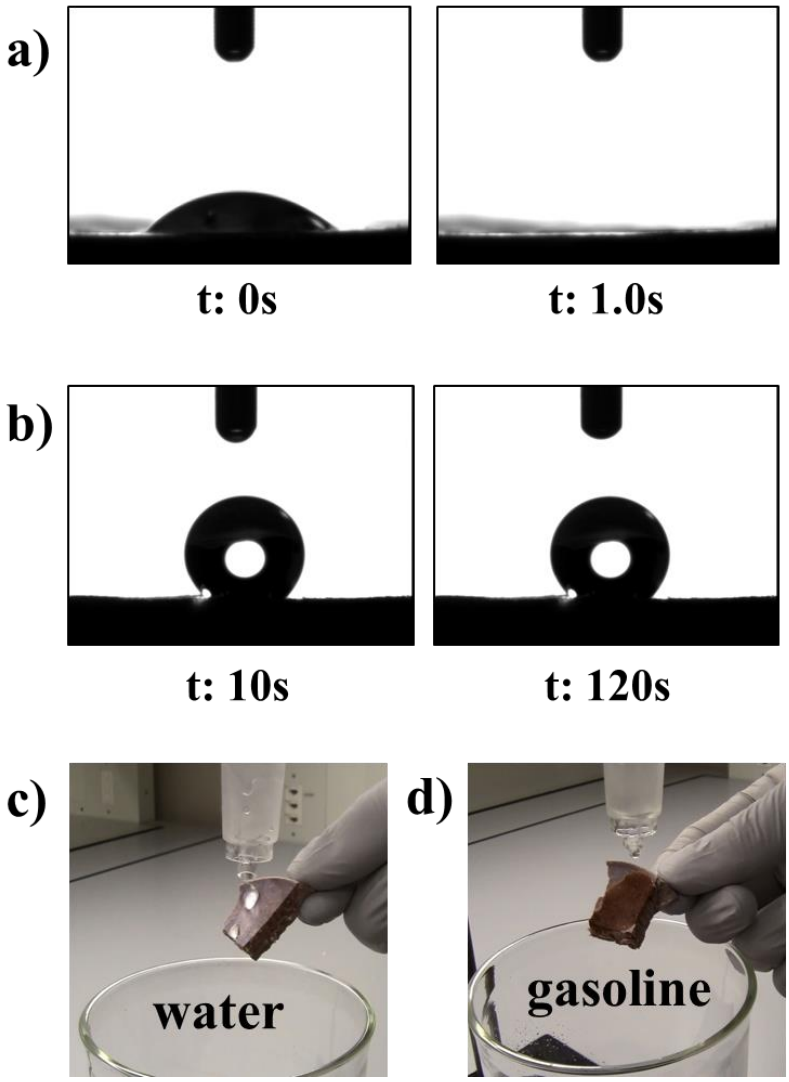

Fig. 5 Water contact angle measurements of the PVA/CNF aerogels: (a) uncoated aerogel and (b) silane-coated aerogel. Optical images of (c) water droplets and (d) gasoline droplets squirted on a piece of silane-coated PVA/CNF aerogel.

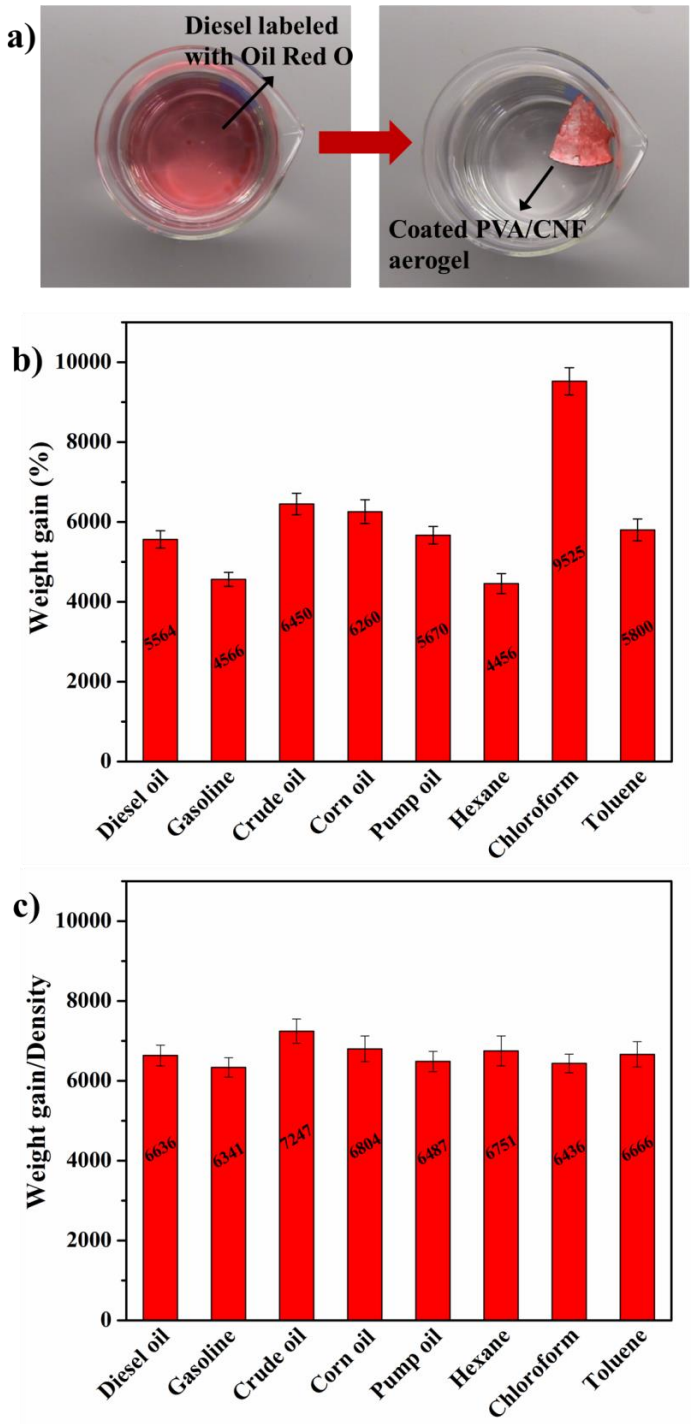

Fig. 6 (a) A layer of diesel on top of the water was absorbed by the silane-coated PVA/CNF aerogel in 90 seconds. The gasoline was labeled with Oil Red O for clarity. (b) Absorption capacities of the PVA/CNF aerogels for various organic solvents and oils as indicated by weight gain. (c) Absorption capacities normalized by the density of the respective oil or organic solvent.

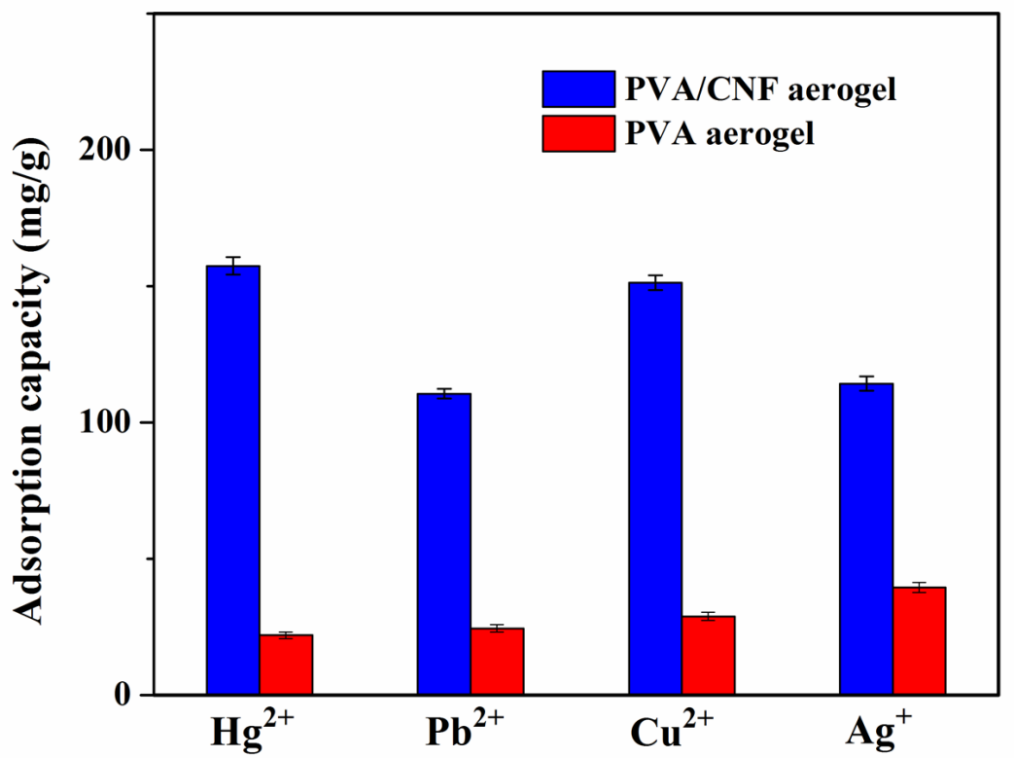

Fig. 7 Heavy metal ion scavenging capabilities of the PVA and PVA/CNF aerogels. The PVA aerogel was used as a control for this test.

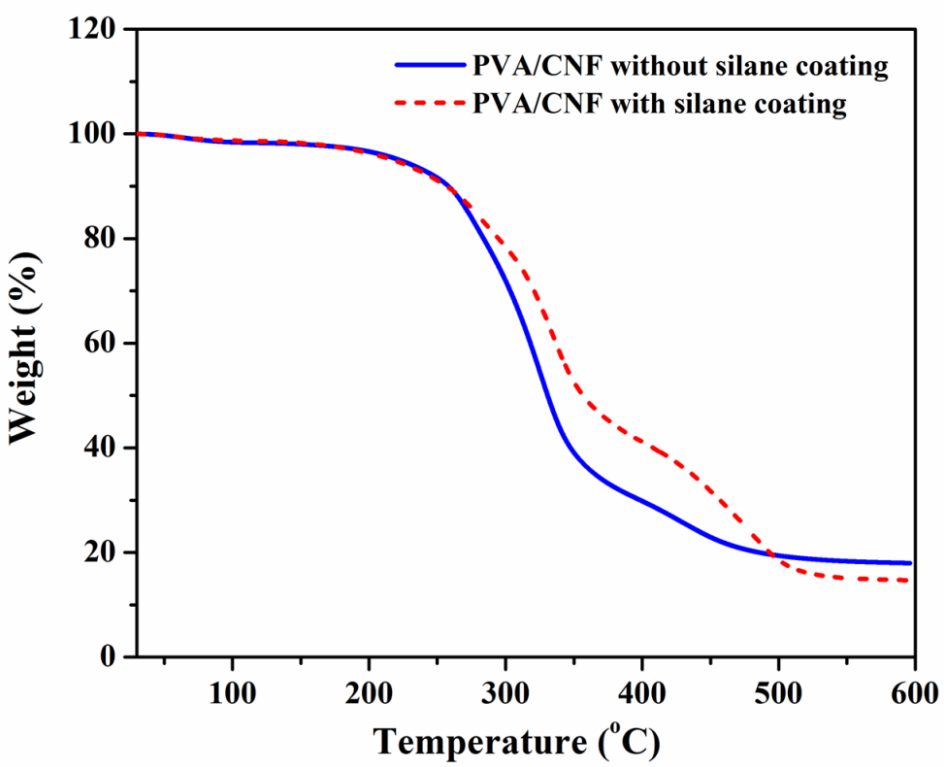

Fig. 8 TGA curves of the PVA/CNF aerogels with and without silane coating.

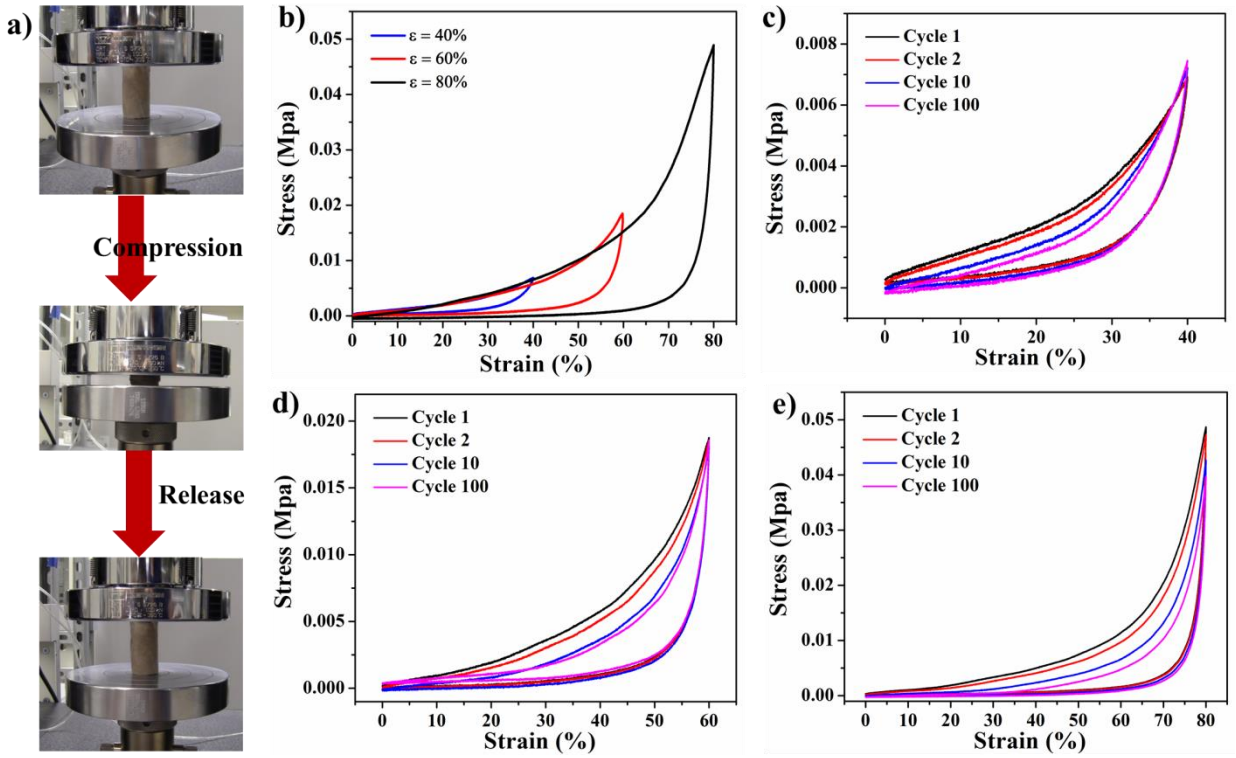

Fig. 9 Mechanical properties of the silane-coated PVA/CNF aerogels. (a) Optical images showing that silane-coated PVA/CNF aerogels recovered their original dimensions after being subjected to more than 80% compression (cf. Movie S4 in the Supporting Information. The sample used to take this movie had a different dimension (i.e., 25 mm in diameter and 55 mm in height) compared to those used for the mechanical tests shown in Fig. 9 (b) to (e). A taller cylindrical sample was used for the movie to demonstrate the elastic properties more clearly.) (b) Compressive stress–strain curves of the PVA/CNF aerogels subjected to different compressive strains; i.e., 40%, 60%, and 80%. Cyclic stress-strain curves of the PVA/CNF aerogels subjected to a compressive strain of (c) 40%, (d) 60%, and (e) 80% over 100 compression cycles.

Table 1 Physical properties of the aerogels with and without silane coating.

Sample	Density ($kg\ m^{-3}$)	Porosity (%)	S_{BET} ($m^2\ g^{-1}$)
uncoated PVA aerogel	11.7	99.08	92±8
coated PVA aerogel	14.2	98.80	76±6
uncoated PVA/CNF aerogel	10.6	99.22	195±18
coated PVA/CNF aerogel	13.0	99.01	172±13

Table 2 Comparison of the absorption capacities of different materials.

Absorption Materials	Absorption capacity ($g\ g^{-1}$)	Reference
Silane-treated PVA/CNF aerogel (this study)	44~96	–
Silicone-manganese oxide nanowire membrane	6~20	2
Spongy graphene	20~86	6
Nonwoven polypropylene	10~16	8
Macroporous butyl rubber	15-23	8
Graphene-based aerogel	28~40	9
Polyurethane/polysiloxane sponge	15~25	12
Microporous conjugated polymers	7~23	47
Polydimethylsiloxane sponge	4~11	48